ACS APPLIED MATERIALS & INTERFACES

Research Article

www.acsami.org

Macroporous ZnO Foams by High Internal Phase Emulsion Technique: Synthesis and Catalytic Activity

Sebastijan Kovačič,*[,†] Alojz Anžlovar,[†] Boštjan Erjavec,[‡] Gregor Kapun,[§] Nadejda B. Matsko,[∥] Majda Žigon,[†] Ema Žagar,[†] Albin Pintar,[‡] and Christian Slugovc[⊥]

[†]National Institute of Chemistry, Laboratory for Polymer Chemistry and Technology, Hajdrihova 19, SI-1001 Ljubljana, Slovenia

[‡]National Institute of Chemistry, Laboratory for Environmental Sciences and Engineering, Hajdrihova 19, SI-1001 Ljubljana, Slovenia

[§]National Institute of Chemistry, Laboratory for Materials Chemistry, Hajdrihova 19, SI-1001 Ljubljana, Slovenia

[∥]Graz Centre for Electron Microscopy (FELMI-ZFE), Steyrergasse 17, A 8010 Graz, Austria

[⊥]Graz University of Technology, Institute for Chemistry and Technology of Materials, Stremayrgasse 9, A-8010 Graz, Austria

Supporting Information

ABSTRACT: Zinc(II) oxide nanoparticles were used for the stabilization of dicyclopentadiene (DCPD)−water-based high internal phase emulsions (HIPEs), which were subsequently cured using ring-opening metathesis polymerization (ROMP). The morphology of the resulting ZnO-pDCPD nanocomposite foams was investigated in correlation to the nanoparticle loading and nanoparticle surface chemistry. While hydrophilic ZnO nanoparticles were found to be unsuitable for stabilizing the HIPE, oleic acid coated, yet hydrophobic ZnO nanoparticles were effective HIPE stabilizers, yielding polymer foams with ZnO nanoparticles located predominately at their surface. These inorganic/organic hybrid foam-materials were subsequently calcined at 550 °C for 15 min to obtain inorganic macroporous ZnO foams with a morphology reminiscent to the original hybrid foam, and a specific surface area of 1.5 m^2 g^{-1}. Longer calcination time (550 °C, 15 h) resulted in a sea urchin like morphology of the ZnO foams, characterized by higher specific surface area of 5.5 m^2 g^{-1}. The latter foam type showed an appealing catalytic performance in the catalytic wet air oxidation (CWAO) process for the destruction of bisphenol A.

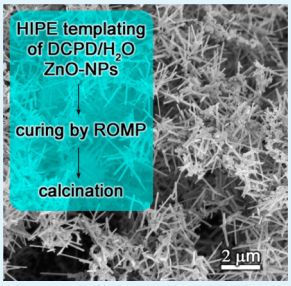

KEYWORDS: *zinc(II) oxide, nanocomposites, polyHIPEs, ROMP, dicyclopentadiene, catalytic wet air oxidation*

1. INTRODUCTION

One of the common synthetic routes to synthesize porous materials involves templates.[1] A special case is templating with the high internal phase emulsions (HIPEs), which evolved as a powerful technique for preparation of open cellular macroporous materials.[2] HIPEs are a special type of emulsions typically with a high internal phase volume fraction exceeding 0.74.[3] Generally, all macro-emulsions, and especially HIPEs, are known to be thermodynamically metastable systems,[4] when stabilized with large amounts (5−50 vol %) of surfactant.[5−7] Over the past few years, particle-stabilized HIPEs (the so-called Pickering HIPEs)[8−10] have become an alternative that replaces hazardous surfactant molecules and, at the same time, provide additional and/or improved properties to the final composite material.[11] Upon curing of HIPEs/Pickering HIPEs, the macroporous monolithic-, bead-, or membrane-like polymers called polyHIPEs/poly(Pickering) HIPEs are obtained with the skeleton being completely inorganic,[12,13] organic[14] or an inorganic−organic hybrid.[15]

Porous inorganic foams are very important materials finding use in diverse technological applications, such as filters, catalysts, absorbers or electrode materials.[16−19] Only a few synthetic routes for porous inorganic foams derived from polyHIPEs were developed so far. Reactive metal alkoxide precursors were emulsified into the continuous phase of HIPEs, from which hybrid polyHIPEs or pure silica-based polyHIPEs were obtained upon polymerization and subsequent calcination.[20] Another way to prepare macroporous inorganic foams is by using the surface-active nanoparticles of the material of interest as stabilizers for Pickering HIPEs. Inorganic nanoparticles alone or in combination with microgel particles[21] or surfactant molecules[22−24] have been already used as stabilizers. Recently, it was demonstrated that TiO_2 and γ-Fe_2O_3/Fe_3O_4 nanoparticles formed Pickering HIPEs, which were upon polymerization calcined in oxygen flow to form the three-dimensional interconnected porous TiO_2[25] or Fe_2O_3[26] monoliths.

Herein, we wish to extend this approach toward semiconducting metaloxides. Among various semiconducting metal salts, ZnO is a technologically important material with a wide range of applications such as in gas sensors,[27] biosensors,[28,29] field-effect transistors,[30] photocatalysis,[31,32] and dye-sensitized solar cells.[33] Numerous efforts have been devoted to the synthesis of ZnO nanostructures[34,35] such as nanorods,[36] nanowires,[37] and nanospheres,[38] however, a fabrication of self-standing, three-dimensional (3D), macroporous ZnO is still

Received: July 30, 2014
Accepted: October 21, 2014
Published: October 21, 2014

Scheme 1. Preparation Protocol of the ZnO-p(DCPD) Nanocomposite and Pure ZnO Foams

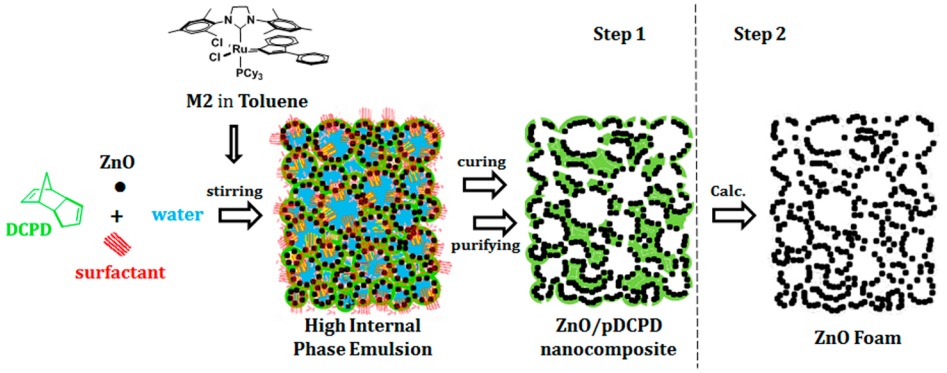

Table 1. Pickering Emulsions' Compositions with Hydrophilic ZnO-NP (80 vol. % Aqueous Phase), Cavity (d_{cav}), and Window Diameters (d_{win})

		$d_{cav} \pm \sigma$ [μm][b]		$d_{win} \pm \sigma$ [μm][b]	
sample	ZnO-NPs [wt %]	small	large	in small cavity	in large cavity
pDCPD_1w[a]	1	8.5 ± 4.0	23 ± 4	1.6 ± 0.7	2.2 ± 1.1
pDCPD_5w[a]	5	10.0 ± 5.5	49 ± 34	1.0 ± 0.6	1.8 ± 0.5
pDCPD_8w[a]	8	9.0 ± 4.5	202 ± 84	1.0 ± 0.5	1.6 ± 0.8

[a]Samples containing ZnO-NPs (nonmodified ZnO). [b]Determined from SEM images of broken samples.

rare.[39,40] To demonstrate the versatility of the Pickering approach and its potential to generate inorganic macroporous foams with functional properties, we herein disclose a straightforward way to produce self-standing macroporous zinc oxide foams derived from ZnO-poly(dicyclopentadiene), ZnO-pDCPD, nanocomposite foams. Moreover, we show an exceptional catalytic performance of ZnO foams within an artificial wastewater cleaning process, the so-called catalytic wet air oxidation (CWAO) process, whereby an aqueous solution of bisphenol A (BPA) is degraded in a continuous-flow trickle-bed reactor.

2. RESULTS AND DISCUSSION

For preparation of macroporous zinc oxide foams a two-step procedure as depicted in Scheme 1 was used. The first step involved the generation of macroporous ZnO-pDCPD nanocomposite foams from the HIPEs that consisted of a mixture of dicyclopentadiene (DCPD; 20 vol %) as a monomer, ZnO-NP (1−30 wt % according to monomer, cf. Table 1) as a stabilizer, and surfactant Pluronic L-121 (7 vol % according to monomer) as a costabilizer. The internal droplet phase was deionized water (80 vol %). This formulation was subsequently cured upon addition of a ring-opening metathesis polymerization initiator (M2, see Figure 1). Two types of ZnO-NPs with an average diameter of 50 nm,[41−43] but different surface properties were tested. Both types of ZnO-NPs were synthesized by a polyol method as described elsewhere.[41] The rather hydrophilic unmodified ZnO nanoparticles (labeled as ZnO-NPs) exhibited a contact angle of 45° for water, whereas the ZnO nanoparticles, surface modified with oleic acid (labeled as OA-ZnO-NPs) were characterized by a contact angle of 103°. It is well-known that the stability of Pickering emulsions is affected by a number of factors (e.g., size, shape and concentration of the particles used, etc.), wherein the particle wettability (often expressed as a contact angle θ at the three phase boundary) is particularly crucial. Wettability is a measure of the extent of wetting the particles by a particular liquid (i.e., how a liquid spreads on the surface of the solid), and is quantified by the contact angle (θ) that the particle forms with the liquid.

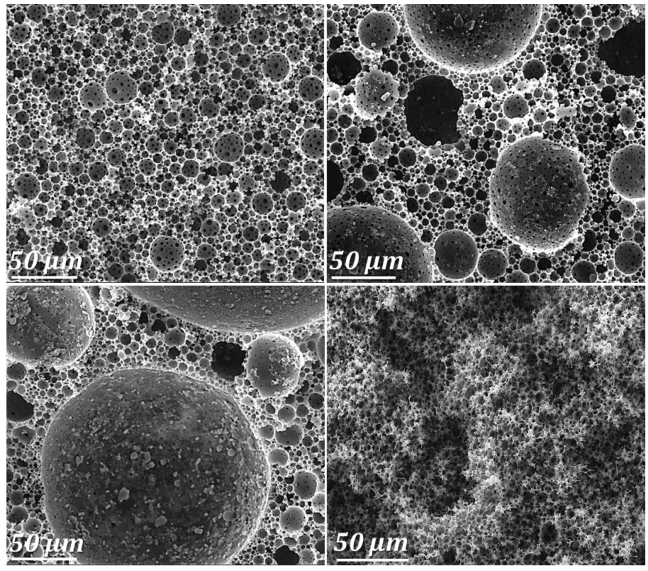

Figure 1. First row from left to right: SEM images of **pDCPD_1w** and **pDCPD_5w** samples; second row from left to right: SEM images of **pDCPD_8w** and **pDCPD_8w_12OA** samples.

Low θ values indicate high wettability (θ_{ow} < 90°; more hydrophilic particles), whereas high θ values are indicative of low wettability (θ_{ow} > 90°; more hydrophobic particles).[44,45] Stable W/O HIPEs (macroscopic evaluation) were obtained with HIPE formulations differing in (hydrophilic) ZnO-NPs loading (1, 5, and 8 wt % according to DCPD), which solidified upon addition of the ROMP-initiator (0.014 mol % of M2 with respect to DCPD, dissolved in 100 μL of toluene),[46] and curing at 80 °C for 4 h. Thus, obtained ZnO-pDCPD nanocomposite foams were purified by Soxhlet extraction with acetone and dried in a desiccator under vacuum. No shrinkage of foams was

dx.doi.org/10.1021/am5050482 | ACS Appl. Mater. Interfaces 2014, 6, 19075−19081

Table 2. Pickering Emulsions Compositions (80 vol. % Aqueous Phase), Cavity (d_{cav}), and Window Diameters (d_{win})

sample	OA-ZnO-NPs [wt %]	OA[b] [wt %]	$d_{cav} \pm \sigma$ [μm][c]	$d_{win} \pm \sigma$ [μm][c]	S_{BET} [m^2 g^{-1}]	skeletal density [g cm^{-3}]
pDCPD_8w_12OA[a]	8	12	6.7 ± 1.6	1.8 ± 0.7		
pDCPD_30w_3OA[a]	30	3	5.0 ± 1.7	1.5 ± 0.8	4.2	1.68
pDCPD_30w_6OA[a]	30	6	5.6 ± 1.6	2.0 ± 0.8	4.0	1.67
pDCPD_30w_12OA[a]	30	12	6.9 ± 1.6	2.4 ± 1.0	3.7	1.77
ZnO foam			2.6 ± 0.7		1.7	5.06
ZnO foam, needle-like structure					5.5	5.06

[a]Samples containing OA-ZnO-NPs (ZnO modified with OA, oleic acid). [b]Oleic acid. [c]Determined from SEM images of broken samples according to ref 26

observed since they retained the shape of the mold. Specimens' microstructure was evaluated by scanning electron microscopy (SEM). For this purpose the specimens were aged, that is, they were exposed to air as described elsewhere[47] to be able to break or grind the samples. SEM analysis revealed open cellular structure in all cases (cf., Figure 1) and a bimodal distribution of cavity size. Both, large and small cavities (cf., Table 1) contain interconnecting pores of size ranging from 1 ± 0.6 μm to 1.6 ± 0.7 μm for small cavities, and from 1.7 ± 0.6 μm to 2.1 ± 1.1 μm for large cavities (the mean cavity and window diameter were determined by SEM image analysis).[48] The observed bimodal cavity size distribution is most probably a consequence of reduced emulsion stability and occurrence of coalescence before polymerization.[49] It seems that the surfactant, used for HIPE stabilization, is preferably adsorbed on the ZnO-NPs surface and, consequently, less surfactant remains at the oil–water interface, thus destabilizing the HIP emulsion. This tentative explanation is supported by the fact that higher ZnO-NPs loadings led to larger cavities, i.e. more intense coalescence occurred before the gel point of the polymerization was reached. Increasing the amount of ZnO-NPs above 8 wt % caused complete phase separation of the emulsion before it was polymerized.

Moreover, previous work on the DCPD/pluronic L-121 system revealed that surfactant loadings below 3 vol % exhibited significant impact on the emulsion stability and, consequently, the cavity size, which increased rapidly with decreasing surfactant amount in the HIPEs below 3 vol %.[50] As confirmed by the energy filtered TEM (EFTEM) and the energy-dispersive X-ray spectroscopy (EDX) of the **pDCPD-8w** sample, no **ZnO-NPs** were found neither on the surface nor in the bulk of the foam skeleton (cf., Supporting Information Figure S1 and S2). Most likely, the ZnO-NPs (or nanoparticle/surfactant aggregates) moved preferentially into the water phase and were subsequently removed during washing the foam.

The ZnO-NPs surface functionalized with oleic acid behave differently. Upon using 8 wt % OA-ZnO-NPs, containing 12 wt % of oleic acid, the anticipated HIPE structure with monodisperse cavity size was obtained (cf., Figure 1). Statistical analysis of SEM micrographs showed the mean cavity and interconnecting pore sizes of 6.7 ± 1.6 and 1.8 ± 0.7 μm in diameter, respectively (cf., Table 2). In this case the OA-ZnO-NPs were found in the foam structure.

For the preparation of macroporus ZnO foams Pickering HIPEs with a high amount of ZnO nanoparticles are needed. Therefore, based on recent experiences with the preparation of Fe_2O_3 foams from FeO_x nanoparticle containing HIPEs,[26] a loading of 30 wt % of OA-ZnO-NPs was chosen. The OA-ZnO-NPs modified with different amounts of oleic acid (i.e., 3, 6, and 12 wt % of OA, cf. Table 2) were used.[51] After polymerization, purification and drying, visually no shrinkage was observed as the nanocomposite foams retained the shape of the mold.

SEM micrographs showed typical polyHIPE interconnected macroporous architecture for samples containing OA-ZnO-NPs (cf. Figure 2). Statistical analysis of SEM micrographs revealed

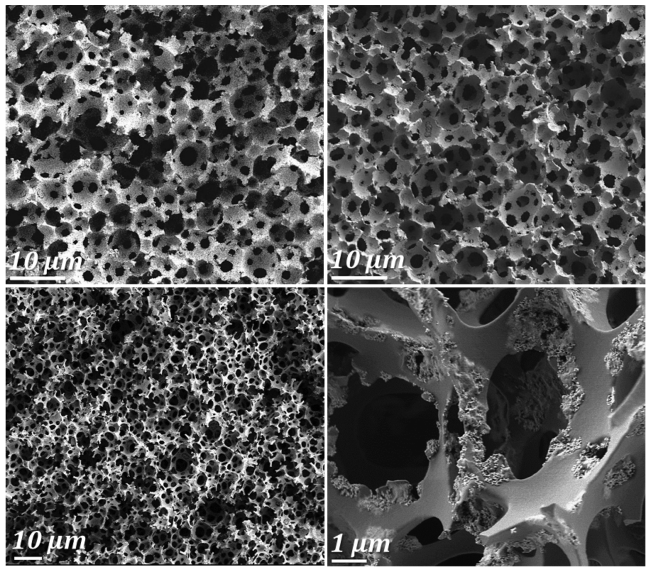

Figure 2. First row from left to right: SEM images of **pDCPD_30w_3OA** and **pDCPD_30w_6OA** samples; second row from left to right: SEM images of **pDCPD_30w_12OA** and **pDCPD_30w_12OA** sample at higher magnification.

that size distribution of cavities and interconnecting pores is polydisperse within the error of standard deviation (10 % of the mean cavity size) as expected. No bimodal cavity-like structure was observed as in the case of unmodified ZnO-NPs. Moreover, high-magnification SEM image of the **pDCPD-30w-12OA** sample showed certain amount of NPs to reside on the surface of the macropores (cf., Figure 2 and Supporting Information Figure S8). STEM investigation of the **pDCPD-30w-12OA** sample revealed the vast majority of all **OA-ZnO-NPs** to be at the pore/polymer interface, while the minor amount was also found in the bulk of the foam skeleton (cf., Supporting Information Figure S12). The results of TGA analysis of the oxidized **pDCPD-30W-3OA**, **pDCPD30W-6OA**, and **pDCPD-30W-12OA** samples revealed the presence of high content of the **OA-ZnO-NPs** in all cases (see details in Supporting Information).

The second step in the preparation protocol, the calcination of the macroporous ZnO/p(DCPD) nanocomposite, was carried out on the **pDCPD-30W-12OA** sample. Specimens were calcined in a Protherm furnace operated under the air at

550 °C for different periods of time (i.e., 15 min and 15 h). Upon calcination, the organic part of the nanocomposite foam was burnt away (as assured by EDX), whereas the inorganic part, that is, ZnO, left over and maintained the nanocomposite's macroscopic structure. However, the macroscopic structure is not particularly stable and thus obtained ZnO-foams are very brittle and disintegrate upon touching. Nevertheless, as evident from Figure 3, the microscopic

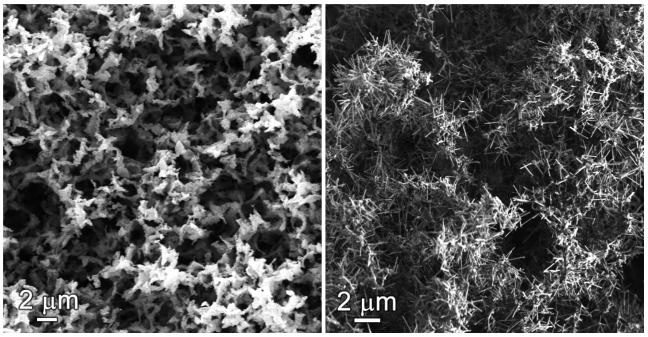

Figure 3. Left: SEM image of ZnO foam with macroporous morphology. Right: SEM image of ZnO foam with needle-like morphology.

structure of the ZnO foam prepared by calcination for 15 min was reminiscent to the original nanocomposite foam's structure (cavity sizes of around 2.6 ± 0.7 μm). In contrast, the ZnO foam calcined for 15 h at 550 °C exhibited a completely different porous structure, i.e. a needle-like morphology reminiscent to sea urchins, as can be clearly seen on the right side of Figure 3. Needle-like morphologies of ZnO have been obtained before using different hydrothermal preparations[52,53] or zinc sources (e.g., zinc acetate).[54,55] In our case, a probable explanation for the formation of the needle-like morphology is that the needle-growth of ZnO occurred from the surface of ZnO nanoparticles, which are capped with the oleate groups following a similar mechanism as described in literature.[55] However, performing the calcination of the nanoparticles as employed for the preparation of the hybrid foams (functionalized and nonfunctionalized with OA) as control experiments at the same conditions (i.e., 15 h at 550°) did not result in the formation of a needle-like ZnO morphology (cf. Supporting Information Figure S11). Accordingly, it can be assumed that the pretreatment (i.e., the chosen HIPE templating process) or the presence of pDCPD during the calcination is responsible for the formation of the needle-like morphology.[56]

Both ZnO-foam samples (annealed for 15 min or 15 h at 550 °C) with different morphologies were further characterized by the X-ray diffraction (XRD) and the electron dispersive spectroscopy (EDS). The XRD pattern showed typical diffraction peaks for polycrystalline zincite at θ = 31.7°, 34.4° 36.2°, 47.5°, and 56.5° (cf., Supporting Information Figure S14), while the EDS spectra showed Zn signals at 1, 8.7, and 9.6 keV, both indicating pure inorganic ZnO foam, formed upon calcination (see details in Supporting Information). However, the EDS spectrum of the ZnO foam annealed for only 15 min indicated the presence of residual organic matter as well. In addition, an increase of specific surface area from 1.6 (for ZnO foam annealed for 15 min) to 5.5 $m^2\ g^{-1}$ (for ZnO foam annealed for 15 h) was found upon calculations using BET theory (cf., Table 2). Only the sample with needle-like morphology (pure ZnO foam) was further examined as a heterogeneous catalyst in the catalytic wet air oxidation (CWAO) process.[57] To the best of our knowledge, this is the first time that ZnO was used in such an application. The catalytic wet air oxidation process is one of the most promising advanced oxidation processes for the removal of hazardous organic compounds from industrial waste waters because of the incorporation of heterogeneous catalysts and its performance at relatively mild conditions as compared to other oxidation processes.[58] Recently, titanate nanotubes (TNTs) were discovered as an efficient catalyst for the removal of organic pollutants represented by bisphenol A (BPA) from aqueous solution without the addition of noble metals.[59] The as-obtained titanate nanotubes, possessing BET specific surface area of 400 $m^2\ g^{-1}$, were found to be stable and resistant to leaching of active ingredient material into the liquid phase during long-term CWAO experiments. Using this system as a benchmark, we tested the ZnO foam disclosed here as a catalyst in the CWAO of aqueous BPA using a three-phase trickle-bed reactor. In contrast to the TNT catalyst, the needle-like ZnO foam exhibited BET specific surface area of only 5 $m^2\ g^{-1}$; however, the catalytic activity of these two transition metal oxides was comparable within the first 2 h of the CWAO process (cf., Figure 4). These results point to an excellent initial ability of the needle-like ZnO foam to catalyze the oxidation of BPA. Catalytic liquid-phase oxidation of aqueous BPA

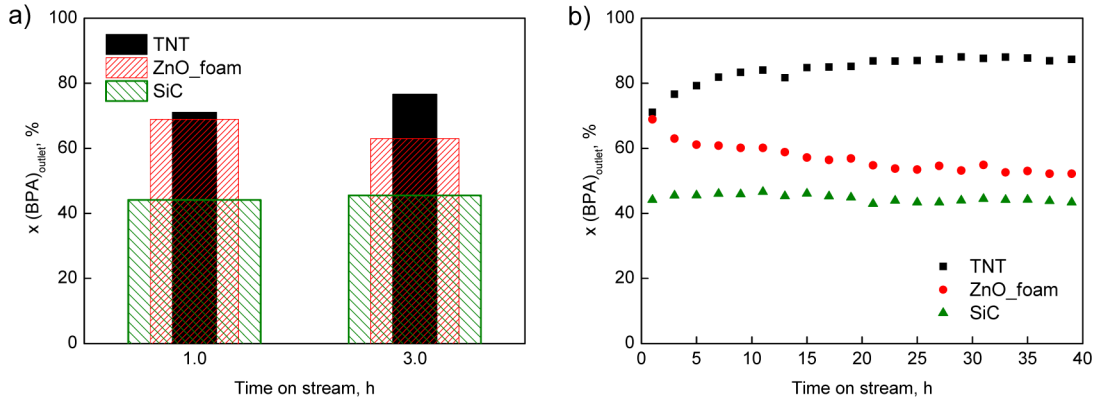

Figure 4. BPA conversion as a function of time on stream (4 (a) and 40 h (b)) over titanate nanotube-based catalyst, ZnO foam and inert SiC, determined by means of HPLC technique. Operating conditions: $p(O_2)$ = 10.0 bar, $\Phi_{vol,L}$ = 0.5 mL min^{-1}, $c(BPA)_{feed}$ = 10.0 mg L^{-1}, m_{cat} = 300 mg, T = 200 °C.

dx.doi.org/10.1021/am5050482 | ACS Appl. Mater. Interfaces 2014, 6, 19075−19081

undergoes a stepwise consecutive/parallel reaction pathway, in which low-chain carboxylic acids (predominantly as a recalcitrant acetic acid) and carbon dioxide are formed via partially oxidized aromatic intermediates. However, the initially observed high catalytic activity started to progressively decrease, reaching a steady-state equilibrium, which still provides a distinct acceleration of the BPA degradation compared to a noncatalyzed, solely thermally induced wet air oxidation process (catalytically inactive and low BET surface area of SiC particles were used for realizing this scenario). The trend in total organic carbon (TOC) conversion was consistent with the trend in BPA conversion determined by HPLC measurements. The liquid-phase samples (withdrawn after 40 h on stream) obtained in the presence of ZnO foam exhibited TOC conversion of 38 wt %, which in comparison to the noncatalytic conversion over SiC particles (20 wt %) confirmed the catalytic activity of ZnO foam. The remaining TOC content in reactor outlet was attributed to recalcitrant aliphatic acids (i.e., acetic, formic and propionic) and trace amounts of p-hydroxyacetophenone (p-HAP), besides unconverted BPA. The observed decrease in catalytic activity cannot be attributed to eventual coking of the catalyst surface, since negligibly small amount of accumulated carbon was detected at the end of the oxidation run. More likely, decreased catalytic activity is a consequence of dissolution of zinc ions into the liquid phase provoked by hydrothermal operating conditions. Since the constant catalytic activity was established after about 20 h on stream (cf., Figure 4), this further alludes that the dissolution of zinc ions occurred from the most active ZnO sites. These results may account for the needle-like structure of macroporous ZnO foam as a potential highly catalytically active material for liquid-phase oxidation of water-soluble organic pollutants, however, the structure stability will have to be considerably improved (e.g., by admixing other transition metal oxides, surface stabilization with coatings, doping, etc.) to meet a long-term steady-state performance.

3. EXPERIMENTAL SECTION

3.1. Materials. Dicyclopentadiene (**DCPD**, Aldrich), Pluronic L121 (poly(ethylene glycol)-*block*-poly(propylene glycol)-*block*-poly-(ethylene glycol, Aldrich), the initiator (H_2IMes)(PCy_3)Cl_2Ru(3-phenyl-indenylid-1-ene) (**M2**, Umicore, H_2IMes = N,N-bis(mesityl) 4,5-dihydroimidazol-2-yl), PCy_3 = tricyclohexylphosphine)), and toluene (p.a. Aldrich) were used as received. ZnO nanoparticles (ZnO-NP, containing 3, 6, and 12 wt % of oleic acid) were prepared according to the literature.[41]

3.2. Preparation of the Materials. The according amounts of monomer DCPD (9.8 mmol, 1.30 g), Pluronic L121, ZnO-NP (cf., Supporting Information Table S1), and toluene (50 μL) were placed in a 3 neck round-bottomed flask equipped with a mechanical stirrer and a dropping funnel. The mixture was stirred at 400 rpm for 5 min and upon continuous stirring deionized water (5.5 mL) was added dropwise at 25 °C over about 1 h. Afterward, the initiator **M2** (1.3 mg, 0.0007 mmol in respect to **DCPD**) dissolved in toluene (0.25 mL) was added and the emulsion was stirred for further 5 min. Subsequently, the emulsion was transferred to appropriate mold (i.e., glass vials) and the filled molds were transferred into a preheated oven operating under air. Curing of the emulsions at 80 °C for 4 h resulted in the formation of white rigid monoliths in all cases. The specimens were purified by Soxhlet extraction with acetone for 24 h and subsequently dried in a desiccator under vacuum (10 mbar) until the constant weight.

3.3. Characterization. TGA measurements were performed with a Netzsch Simultaneous Thermal Analyzer STA 449C (crucibles: aluminum from Netzsch). An oxygen flow of 50 mL min^{-1} was used in combination with a protective flow of helium of 8 mL min^{-1}. The heating rate until a final temperature of 550 °C was 10 °C min^{-1}.

Morphology investigations were performed using scanning electron microscopy. SEM images were taken on a Field emission electron microscope Ultra+ (Carl Zeiss) equipped with energy dispersive spectrometer SDD X-Max 50 (Oxford Instruments). Piece of the each sample was mounted on a carbon tab for better conductivity and thin layer of gold was sputtered on samples surface prior to scanning analysis. Evaluation of the feature sizes was done according to ref 46.

For TEM analysis, samples were embedded in Araldite/Epon embedding mixture, which was composed of 49% w/w Araldite/Epon stock solution, 49% w/w hardener DDSA (Fluka) and 2% w/w accelerator DMP-30 (Fluka). Infiltration was performed stepwise (impregnation at room temperature for 24 h, and polymerization at 50 °C for 72 h). Embedded samples were sectioned using Leica Ultracut ultramicrotome to a thickness between 70 and 120 nm. All EFTEM experiments were acquired in TEM mode. For the calculation of elemental distribution images, a jump ratio method was used. STEM micrographs of the nanocomposites were taken on a Zeiss Supra 35 VP at an acceleration voltage of 20.0 kV and working distance of 4.5−5 mm using a STEM electron detector.

BET specific surface area, total pore volume and average pore width of the ZnO foam catalysts were determined from the adsorption and desorption isotherms of N_2 at 196 °C using a Micromeritics TriStar II 3020 instrument. Prior to characterization the samples were degassed under N_2 stream (purity 6.0) using a programmed bilevel heating, with the first heating stage at 90 °C for 60 min, followed by the second heating stage at 180 °C for 240 min. The heating rate was set to 10 °C min^{-1} for both heating stages. The specific surface area of the samples was calculated by applying the BET theory to the nitrogen adsorption data within the 0.06−0.30 P/P_0 range. Pore-size distributions were calculated from the desorption branch of the corresponding nitrogen isotherms, applying BJH method.

XRD patterns of ZnO foam were characterized by a wide-angle X-ray diffraction (XRD) on a Siemens D-5000 diffractometer with a Cu anode as the X-ray source. X-ray diffractograms were measured at 25 °C in the 2θ range from 2 to 60° with a step of 0.04° and step time of 100 s.

CWAO experiments were performed in a Microactivity-Reference unit (PID Eng & Tech, Spain), which is a fully automated and computer-controlled continuous-flow trickle-bed reactor. The oxidation took place in a tubular reactor (Autoclave Engineers, USA), made of a 305 mm (length) × 9 mm (inner diameter) Hastelloy C-276 tube and was integrated within the hot box and heated with a reactor furnace (for details see Supporting Information).

Undegraded BPA in acquired liquid-phase samples was determined by high-performance liquid chromatography (HPLC) in the isocratic analytical mode, using a 100 mm × 4.6 mm BDS Hypersil C18 2.4 μm column, thermostated at 30 °C and equipped with a universal column protection system. The mobile phase was composed of methanol and ultrapure water (70:30 volume ratio), and was introduced into the system with a flow rate of 0.5 mL min^{-1}, while an UV detection was fixed at λ = 210 nm.

4. CONCLUSIONS

In summary, a two-step synthetic route to obtain three-dimensional macroporous ZnO materials via a Pickering high internal phase emulsion (HIPE) templating approach is described. We have demonstrated the versatility of combining ZnO nanoparticles, surface functionalized by oleic acid and surfactant molecules to form stable HIPEs that yield, upon polymerization, open porous nanocomposite foams, which can be further calcined to yield macroporous ZnO. Moreover, by tuning the time of calcination at a given temperature (550 °C) two different morphologies of macroporous ZnO foam were obtained, that is, an open porous and a needle-like morphology. The ZnO of the later morphology was found to be only formed upon calcination of the ZnO/p(DCPD) nanocomposite while

calcination of the pure ZnO nanopraticles under the same conditions did not result in a similar morphology. The needle-like ZnO foam, exhibiting a specific surface area of 5.5 m^2 g^{-1}, was further tested as the heterogeneous catalyst in the catalytic wet air oxidation (CWAO) process for the destruction of bisphenol A in aqueous medium. Preliminary catalytic experiments reveal excellent initial catalytic activity of this ZnO material in the CWAO, although it is characterized by a 40 times lower specific surface area as compared to similarly performing metal oxide catalysts used up to now.

■ ASSOCIATED CONTENT

Supporting Information

Experimental details and additional SEM, STEM (EFTEM) and EDX images, N_2 physisorption isotherms, and CWAO data are available. This material is available free of charge via the Internet at http://pubs.acs.org.

■ AUTHOR INFORMATION

Corresponding Author

*E-mail: sebastijan.kovacic@ki.si.

Notes

The authors declare no competing financial interest.

■ ACKNOWLEDGMENTS

The authors gratefully acknowledge the financial support of the Ministry of Higher Education, Science and Technology of the Republic of Slovenia, and the Slovenian Research Agency (Program P2-0145). The authors wish to thank Renata Kaplan for her assistance with the CWAO experiments and UMICOR for the gift of Ru complexes.

■ REFERENCES

(1) Wu, D.; Xu, F.; Sun, B.; Fu, R.; He, H.; Matyjaszewski, K. Design and Preparation of Porous Polymers. *Chem. Rev.* **2012**, *112*, 3959−4015.
(2) Silverstein, M. PolyHIPEs: Recent Advances in Emulsion-Templated Porous Polymers. *Prog. Polym. Sci.* **2014**, *39*, 199−234.
(3) Cameron, N. R.; Krajnc, P.; Silverstein, M. S. Colloidal Templating. In *Porous Polymers*; Silverstein, M. S.; Cameron, N. R. Hillmyer, M. A., Eds.; John Wiley & Sons, Inc.: Hoboken, NJ, 2011.
(4) Esquena, J.; Solans, C. *Emulsions and Emulsion Stability*; Marcel Dekker Inc.: Amsterdam, 2006.
(5) Williams, J. M. High Internal Phase Water-in-Oil Emulsions: Influence of Surfactants and Cosurfactants on Emulsion Stability and Foam Quality. *Langmuir* **1991**, *7*, 1370−1377.
(6) Cameron, N. R.; Sherington, D. C. High Internal Phase Emulsions (HIPEs) Structure, Properties and Use in Polymer Preparation. *Adv. Polym. Sci.* **1996**, *126*, 163−214.
(7) Zhang, H. F.; Cooper, A. I. Synthesis and Applications of Emulsion-Templated Porous Materials. *Soft Matter* **2005**, *1*, 107−113.
(8) Ikem, V. O.; Menner, A.; Bismarck, A. High Internal Phase Emulsions Stabilized Solely by Functionalized Silica Particles. *Angew. Chem., Int. Ed.* **2008**, *47*, 8277−8279.
(9) Menner, A.; Ikem, V.; Salgueiro, M.; Shaffer, M. S. P.; Bismarck, A. High Internal Phase Emulsion Templates Solely Stabilised by Functionalised Titania Nanoparticles. *Chem. Commun.* **2007**, 4274−4276.
(10) Gurevitch, I.; Silverstein, M. S. Polymerized Pickering HIPEs: Effects of Synthesis Parameters on Porous Structure. *J. Polym. Sci., Part A-1: Polym. Chem.* **2010**, *48*, 1516−1525.
(11) Zhang, H.; Liu, Y.; Yao, D.; Yang, B. Hybridization of Inorganic Nanoparticles and Polymers to Create Regular and Reversible Self-Assembly Architectures. *Chem. Soc. Rev.* **2012**, *41*, 6066−6088.
(12) Imhof, A.; Pine, D. J. Ordered Macroporous Materials by Emulsion Templating. *Nature* **1997**, *389*, 948−951.
(13) Zhang, H.; Hardy, G. C.; Khimyak, Y. Z.; Rosseinsky, M. J.; Cooper, A. I. Synthesis of Hierarchically Porous Silica and Metal Oxide Beads Using Emulsion-Templated Polymer Scaffolds. *Chem. Mater.* **2004**, *16*, 4245−4256.
(14) Pulko, I.; Krajnc, P. High Internal Phase Emulsion Templating—A Path to Hierarchically Porous Functional Polymers. *Macromol. Rapid Commun.* **2012**, *33*, 1731−1746.
(15) Brun, N.; Ungureanu, S.; Deleuze, H.; Backov, R. Hybrid Foams, Colloids and Beyond: From Design to Applications. *Chem. Soc. Rev.* **2011**, *40*, 771−788.
(16) Krawiec, P.; DeCola, P. L.; Gläser, R.; Weitkamp, J.; Kaskel, S. Oxide Foams For the Synthesis of High-Surface-Area Vanadium Nitride Catalysts. *Adv. Mater.* **2006**, *18*, 505−508.
(17) Yu, Y.; Chen, C. H.; Shui, J. L.; Xie, S. Nickel-Foam-Supported Reticular CoO-Li_2O Composite Anode Materials for Lithium Ion Batteries. *Angew. Chem., Int. Ed.* **2005**, *44*, 7085−7089.
(18) Xu, J.; White, T.; Li, P.; He, C.; Han, Y. F. Hydroxyapatite Foam as a Catalyst for Formaldehyde Combustion at Room Temperature. *J. Am. Chem. Soc.* **2010**, *132*, 13172−13173.
(19) Hung, T. C.; Huang, J. S.; Wang, Y. W.; Lin, K. Y. Inorganic Polymeric Foam as a Sound Absorbing and Insulating Material. *Constr. Build. Mater.* **2014**, *50*, 328−334.
(20) Silverstein, M. S. Emulsion-Templated Porous Polymers: A Retrospective Perspective. *Polymer* **2014**, *55*, 304−320.
(21) Li, Z. F.; Wei, X. L.; Ming, T. A.; Wang, J. F.; Ngai, T. Dual Templating Synthesis of Hierarchical Porous Silica Materials with Three Orders of Length Scale. *Chem. Commun.* **2010**, *46*, 8767−8769.
(22) Ikem, V. O.; Menner, A.; Bismarck, A. Tailoring the Mechanical Performance of Highly Permeable Macroporous Polymers Synthesized via Pickering Emulsion Templating. *Soft Matter* **2011**, *7*, 6571−6577.
(23) Wang, S.; Zhang, Z.; Liu, H.; Zhang, W.; Qian, Z.; Wang, B. One-Step Synthesis of Manganese Dioxide/Polystyrene Nanocomposite Foams via High Internal Phase Emulsion and Study of Their Catalytic Activity. *Colloid Polym. Sci.* **2010**, *288*, 1031−1039.
(24) Kovačič, S.; Ferk, G.; Drofenik, M.; Krajnc, P. Nanocomposite PolyHIPEs with Magnetic Nanoparticles: Preparation and Heating. *React. Funct. Polym.* **2012**, *72*, 955−961.
(25) Li, X.; Sun, G.; Li, Y.; Yu, J. C.; Wu, J.; Ma, G. H.; Ngai, T. Porous TiO_2 Materials Through Pickering High-Internal Phase Emulsion Templating. *Langmuir* **2014**, *30*, 2676−2683.
(26) Kovačič, S.; Matsko, N. B.; Ferk, G.; Slugovc, C. Macroporous Poly(Dicyclopentadiene) $\gamma Fe_2O_3/Fe_3O_4$ Nanocomposite Foams by High-Internal Phase Emulsion Templating. *J. Mater. Chem. A* **2013**, *1*, 7971−7978.
(27) Fulati, A.; Ali, S. M. U.; Asif, M. H.; Alvi, N. U.; Willander, M.; Brannmark, C.; Stralfors, P.; Börjesson, S. I.; Elinder, F.; Danielsson, B. An Intracellular Glucose Biosensor Based on Nanoflake ZnO. *Sens. Actuators, B* **2010**, *150*, 673−680.
(28) Gu, B. X.; Xu, C. X.; Zhu, G. P.; Liu, S. Q.; Chen, L. Y.; Li, X. S. Tyrosinase Immobilization on ZnO Nanorods for Phenol Detection. *J. Phys. Chem. B* **2009**, *113*, 377−381.
(29) Gu, B. X.; Xu, C. X.; Zhu, G. P.; Liu, S. Q.; Chen, L. Y.; Wang, M. L.; Zhu, J. J. Layer by Layer Immobilized Horseradish Peroxidase on Zinc Oxide Nanorods for Biosensing. *J. Phys. Chem. B* **2009**, *113*, 6553−6557.
(30) Fan, Z. Y.; Wang, D. W.; Chang, P. C.; Tseng, W. Y.; Lu, J. ZnO Nanowire Field Effect Transistor and Oxygen Sensing Property. *Appl. Phys. Lett.* **2004**, *85*, 5923−5925.
(31) Hong, R. Y.; Li, J. H.; Chen, L. L.; Liu, D. Q.; Li, H. Z.; Zheng, Y. Synthesis, Surface Modification and Photocatalytic Property of ZnO Nanoparticles. *Powder Technol.* **2009**, *189*, 426−432.
(32) Tian, Q.; Li, J.; Xie, Q.; Wang, Q. Morphology-Tuned Synthesis of Arrayed One-Dimensional ZnO Nanostructures from $Zn(NO_3)_2$ and Dimethylamine Borane Solutions and Their Photoluminescence and Photocatalytic Properties. *Mater. Chem. Phys.* **2012**, *132*, 652−658.
(33) Han, J. B.; Fan, F. R.; Xu, C.; Lin, S. S.; Wei, M.; Duan, X.; Wang, Z. L. ZnO Nanotube-Based Dye-Sensitized Solar Cell and Its

Application in Self-Powered Devices. *Nanotechnology* **2010**, *21*, 405203−405210.
(34) Kołodziejczak-Radzimska, A.; Jesionowski, T. Zinc Oxide—From Synthesis to Application: A Review. *Materials* **2014**, *7*, 2833−2881.
(35) Anžlovar, A.; Ksenija, K.; Orel, Z. C.; Žigon, M. Impact of Inorganic Hydroxides on ZnO Nanoparticle Formation and Morphology. *Cryst. Growth Des.* **2014**, *14*, 4262−4269.
(36) Marlinda, A. R.; Huang, N. M.; Muhamad, M. R.; Anamt, M. N.; Chang, B. Y. S.; Yusoff, N.; Harrison, I.; Lim, H. N.; Chia, C. H.; Vijay Kumar, S. Highly Efficient Preparation of ZnO Nanorods Decorated Reduced Graphene Oxide Nanocomposites. *Mater. Lett.* **2012**, *80*, 9−12.
(37) Lee, Y. J.; Sounart, T. L.; Liu, J.; Spoerke, E. D.; McKenzie, B. B.; Hsu, J. W. P. Tunable Arrays of ZnO Nanorods and Nanoneedles via Seed Layer and Solution Chemistry. *Cryst. Growth Des.* **2008**, *8*, 2036−2040.
(38) Zhang, P.; Xu, F.; Navrotsky, A.; Lee, J. S.; Kim, S. T.; Liu, J. Surface Enthalpies of Nanophase ZnO with Different Morphologies. *Chem. Mater.* **2007**, *19*, 5687−5693.
(39) Yan, X.; Tong, X.; Wang, J.; Gong, C.; Zhang, M.; Liang, L. Controllable Synthesis of Three-Dimensional Hierarchical Porous ZnO Film with Mesoporous Nanowalls. *Mater. Lett.* **2013**, *92*, 165−168.
(40) Xu, L.; Zheng, G.; Wang, J.; Lai, M.; Miao, J.; Xian, F.; Gu, F.; Sun, T. Leaf-Like ZnO Nanostructure and Its Excellent Photocatalytic Activity. *Mater. Lett.* **2014**, *122*, 1−4.
(41) Anžlovar, A.; Kogej, K.; Orel, Z. C.; Žigon, M. Polyol Mediated Nano Size Zinc Oxide and Nanocomposites with Poly(Methyl Methacrylate). *eXPRESS Polym. Lett.* **2011**, *5*, 604−619.
(42) Anžlovar, A.; Orel, Z. C.; Kogej, K.; Žigon, M. Polyol-Mediated Synthesis of Zinc Oxide Nanorods and Nanocomposites with Poly(Methyl Methacrylate). *J. Nanomater.* **2012**, 760872−760881.
(43) Anžlovar, A.; Crnjak Orel, Z.; Žigon, M. Poly(Methyl Methacrylate) Composites Prepared by In Situ Polymerization Using Organophillic Nano-to-Submicrometer Zinc Oxide Particles. *Eur. Polym. J.* **2010**, *46*, 1216−1224.
(44) Aveyard, R.; Binks, B. P.; Clint, J. H. Emulsions Stabilised Solely by Colloidal Particles. *Adv. Colloid Interface Sci.* **2003**, *100*, 503−546.
(45) Menner, A.; Ikem, V.; Bismarck, A. Particle Stabilised High Internal Phase Emulsions, Patent WO/2009/013500.
(46) Leitgeb, A.; Wappel, J.; Urbina-Blanco, C. A.; Strasser, S.; Wappl, S.; Cazin, C. S. J.; Slugovc, C. Two Commercially Available Initiators for the Retarded Ring-Opening Metathesis Polymerization of Dicyclopentadiene. *Monatsh. Chem.* **2014**, DOI: 10.1007/s00706-014-1249-y.
(47) Kovačič, S.; Jeřabek, K.; Krajnc, P.; Slugovc, C. Ring Opening Metathesis Polymerisation of Emulsion Templated Dicyclopentadiene Giving Open Porous Materials with Excellent Mechanical Properties. *Polym. Chem.* **2012**, *3*, 325−328.
(48) Barbetta, A.; Cameron, N. R. Morphology and Surface Area of Emulsion-Derived (PolyHIPE) Solid Foams Prepared with Oil-Phase Soluble Porogenic Solvents: Span 80 as Surfactant. *Macromolecules* **2004**, *37*, 3188−3201.
(49) Cameron, N. R.; Sherrington, D. C.; Albiston, L.; Gregory, D. P. Study of the Formation of the Open-Cellular Morphology of Poly(Styrene/Divinylbenzene) PolyHIPE Materials by Cryo-SEM. *Colloid Polym. Sci.* **1996**, *274*, 592−595.
(50) Kovačič, S.; Matsko, N. B.; Jeřabek, K.; Krajnc, P.; Slugovc, C. On the Mechanical Properties of HIPE Templated Macroporous Poly(Dicyclopentadiene) Prepared with Low Surfactant Amounts. *J. Mater. Chem. A* **2013**, *1*, 487−490.
(51) Thermogravimetric Analysis (TGA) revealed the total content of oleic acid attached to the NP surfaces to e 4.1, 7.0, and 11.7 wt % (Supporting Information, Figure S1), which is in a good agreement with the amount of OA used during modification.
(52) Qu, J.; Yang, Y.; Wu, Q.; Coxon, P. R.; Liu, Y.; He, X.; Xi, K.; Yuana, N.; Ding, J. Hedgehog-Like Hierarchical ZnO Needle-Clusters With Superior Electron Transfer Kinetics for Dye-Sensitized Solar Cells. *RSC Adv.* **2014**, *4*, 11430−11437.
(53) Panda, S. K.; Singh, N.; Pal, S.; Jacob, C. Thickness Dependent Growth of Needle-like and Flower-like ZnO Nanostructures. *J. Mater. Sci.: Mater. Electron.* **2009**, *20*, 771−775.
(54) Ledwith, D.; Pillai, S. C.; Watson, G. W.; Kelly, J. M. Microwave Induced Preparation of A-Axis Oriented Double-Ended Needle-Shaped ZnO Microparticles. *Chem. Commun.* **2004**, 2294−2295.
(55) Feng, W.; Chen, J.; Hou, C. Y. Growth and Characterization of ZnO Needles. *Appl. Nanosci.* **2014**, *4*, 15−18.
(56) Klingshirn, C. ZnO: Material, Physics and Applications. *ChemPhysChem* **2007**, *8*, 782−803.
(57) Owing to the non-negligible content of organic matter, which could be decomposed at 200 °C (CWAO reaction temperature) and deposited on the surface of the low-temperature reactor vital parts, such as liquid−gas separator and level controller, causing malfunctions of these parts the ZnO foam prepared upon 15 min annealing at 550 °C was not tested.
(58) Bistan, M.; Tišler, T.; Pintar, A. Catalytic and Photocatalytic Oxidation of Aqueous Bisphenol A Solutions: Removal, Toxicity, and Estrogenicity. *Ind. Eng. Chem. Res.* **2012**, *51*, 8826−8834.
(59) Erjavec, B.; Kaplan, R.; Djinović, P.; Pintar, A. Catalytic Wet Air Oxidation of Bisphenol A Model Solution in a Trickle-Bed Reactor Over Titanate Nanotube-Based Catalysts. *Appl. Catal., B* **2013**, *132−133*, 342−352.